EMERGING INFECTIONS

Broad-spectrum antiviral GS-5734 inhibits both epidemic and zoonotic coronaviruses

Timothy P. Sheahan,[1]* Amy C. Sims,[1]* Rachel L. Graham,[1] Vineet D. Menachery,[1] Lisa E. Gralinski,[1] James B. Case,[2] Sarah R. Leist,[1] Krzysztof Pyrc,[3] Joy Y. Feng,[4] Iva Trantcheva,[4] Roy Bannister,[4] Yeojin Park,[4] Darius Babusis,[4] Michael O. Clarke,[4] Richard L. Mackman,[4] Jamie E. Spahn,[4] Christopher A. Palmiotti,[4] Dustin Siegel,[4] Adrian S. Ray,[4] Tomas Cihlar,[4] Robert Jordan,[4] Mark R. Denison,[5†] Ralph S. Baric[1†]

Emerging viral infections are difficult to control because heterogeneous members periodically cycle in and out of humans and zoonotic hosts, complicating the development of specific antiviral therapies and vaccines. Coronaviruses (CoVs) have a proclivity to spread rapidly into new host species causing severe disease. Severe acute respiratory syndrome CoV (SARS-CoV) and Middle East respiratory syndrome CoV (MERS-CoV) successively emerged, causing severe epidemic respiratory disease in immunologically naïve human populations throughout the globe. Broad-spectrum therapies capable of inhibiting CoV infections would address an immediate unmet medical need and could be invaluable in the treatment of emerging and endemic CoV infections. We show that a nucleotide prodrug, GS-5734, currently in clinical development for treatment of Ebola virus disease, can inhibit SARS-CoV and MERS-CoV replication in multiple in vitro systems, including primary human airway epithelial cell cultures with submicromolar IC_{50} values. GS-5734 was also effective against bat CoVs, prepandemic bat CoVs, and circulating contemporary human CoV in primary human lung cells, thus demonstrating broad-spectrum anti-CoV activity. In a mouse model of SARS-CoV pathogenesis, prophylactic and early therapeutic administration of GS-5734 significantly reduced lung viral load and improved clinical signs of disease as well as respiratory function. These data provide substantive evidence that GS-5734 may prove effective against endemic MERS-CoV in the Middle East, circulating human CoV, and, possibly most importantly, emerging CoV of the future.

INTRODUCTION

The genetically diverse coronavirus (CoV) family, currently composed of four genogroups [1 (alpha), 2 (beta), 3 (gamma), and 4 (delta)], infects birds and a variety of mammals. Thus far, only CoV groups 1 and 2 are known to infect humans. Although CoV replication machinery exhibits substantial proofreading activity, replication of viral genomic RNA is inherently error-prone, driving the existence of genetically related yet diverse quasi-species (*1*). Most CoV strains are narrow in their host range, but zoonotic CoVs have a proclivity to jump into new host species (*2*). Severe acute respiratory syndrome CoV (SARS-CoV) and Middle East respiratory syndrome CoV (MERS-CoV) are recent examples of newly emerging CoV that caused severe disease in immunologically naïve human populations. SARS-CoV emerged in Guangdong, China in 2002 and, with the aid of commercial air travel, spread rapidly throughout the globe, causing more than 8000 cases with 10% mortality (*2*). In 2012, it was discovered that MERS-CoV evolved to infect humans through bats by way of an intermediate camel host, causing more than 1700 cases with almost 40% mortality and, like SARS-CoV, air travel has fueled global spread to 27 countries (*2*). MERS-CoV is endemic in the Middle East, and serologic studies in the Kingdom of Saudi Arabia and Kenya suggest fairly frequent infections in humans (>45,000 persons) (*3*, *4*). The SARS-CoV epidemic ended over a decade ago, but several SARS-like CoVs have been isolated from bats that efficiently use the human angiotensin-converting enzyme 2 receptor, replicate to high titer in primary human airway cells, and are resistant to existing therapeutic antibodies and vaccines (*5*, *6*). With increasing overlap of human and wild animal ecologies, the potential for novel CoV emergence into humans is great (*2*). Broad-spectrum CoV therapies capable of inhibiting known human CoV would address an immediate unmet medical need and could be an invaluable treatment in the event of novel CoV emergence in the future.

Currently, there are no approved specific antiviral therapies for CoV in humans. Attempts made to treat both SARS-CoV and MERS-CoV patients with approved antivirals (that is, ribavirin and lopinavir-ritonavir) and immunomodulators (that is, corticosteroids, interferons, etc.) have not been effective in randomized controlled trials (*7*). Clinical development of effective CoV-specific direct-acting antivirals (DAAs) has been elusive, although there are several conserved druggable CoV enzyme targets including 3C-like protease, papain-like protease, and nonstructural protein 12 (nsp12) RNA-dependent RNA polymerase (RdRp) (*7*). In 2016, Warren *et al.* reported the in vivo antiviral efficacy of a small-molecule monophosphoramidate prodrug of an adenosine analog, GS-5734, against Ebola virus in nonhuman primates (*8*). Because the mechanism of action of GS-5734 for Ebola virus is the inhibition of the viral RdRp and previous work had suggested weak activity of the nucleoside component of GS-5734 against SARS-CoV (*9*), we sought to assess the antiviral potency and breadth of activity of GS-5734 against a diverse panel of human and zoonotic CoV.

RESULTS

GS-5734 prevents SARS-CoV and MERS-CoV replication in human airway epithelial cells

GS-5734 is a prodrug that requires metabolism by the host cell to the pharmacologically active triphosphate (TP) to inhibit virus replication

[1]Department of Epidemiology, University of North Carolina at Chapel Hill, Chapel Hill, NC 27599, USA. [2]Department of Pathology, Microbiology, and Immunology, Vanderbilt University Medical Center, Nashville, TN 37232, USA. [3]Department of Microbiology, Faculty of Biochemistry, Biophysics, and Biotechnology, Jagiellonian University, Krakow, Poland. [4]Gilead Sciences Inc., Foster City, CA 94404, USA. [5]Division of Infectious Diseases, Department of Pediatrics and Department of Pathology, Microbiology, and Immunology, Vanderbilt University Medical Center, Nashville, TN 37232, USA.
*These authors contributed equally to this work.
†Corresponding author. Email: mark.denison@vanderbilt.edu (M.R.D.); rbaric@email.unc.edu (R.S.B.)

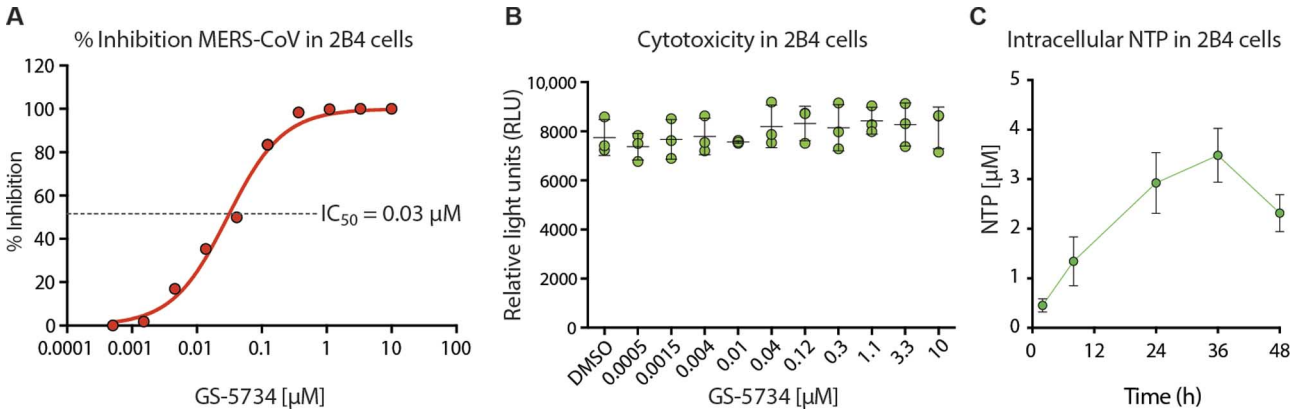

Fig. 1. MERS-CoV antiviral efficacy, toxicity, and metabolism of GS-5734 in 2B4 cells. (**A**) Mean percent inhibition of MERS-CoV replication by GS-5734. 2B4 cells were infected in triplicate with MERS-CoV nanoluciferase (nLUC) at a multiplicity of infection (MOI) of 0.08 in the presence of varying concentrations of GS-5734 for 48 hours, after which replication was measured through quantitation of MERS-CoV–expressed nLUC. (**B**) Cytotoxicity in 2B4 cells treated similarly to that in (A). Viability was measured via CellTiter-Glo. Data for (A) and (B) are representative of three independent experiments. DMSO, dimethyl sulfoxide. (**C**) Measurement of intracellular nucleotide triphosphate (NTP) in 2B4 cells. In three independent experiments, triplicate wells of cells were treated with 1 μM GS-5734 and harvested over time to measure NTP via liquid chromatography–mass spectrometry (LC-MS).

(*9*). To determine whether GS-5734 could inhibit replication of highly pathogenic human CoV, we first evaluated antiviral activity and cytotoxicity in the continuous human lung epithelial cell line Calu-3 2B4 (2B4) (*10*). GS-5734 inhibited MERS-CoV replication in 2B4 cells with an average half-maximum inhibitory concentration (IC_{50}) value of 0.025 μM (Fig. 1A and fig. S1). We did not observe any measureable cytotoxicity at concentrations of up to 10 μM (Fig. 1B and fig. S1), thus demonstrating that the 50% cytotoxic concentration (CC_{50}) for GS-5734 is in excess of 10 μM (CC_{50}/IC_{50} = therapeutic index, >400) in 2B4 cells. With incubation of 1 μM GS-5734, the average intracellular concentration of the pharmacologically active TP of GS-5734 in 2B4 was 2.79 μM during the 48-hour treatment (Fig. 1C). Together, these results suggest that substantial inhibition of CoV replication will be achieved at low micromolar concentrations of the TP in the lung.

Primary human airway epithelial (HAE) cell cultures are among the most biologically relevant in vitro models of the lung, recapitulating the cellular complexity and physiology of the human conducting airway (*11*). We assessed the antiviral activity of GS-5734 against SARS-CoV and MERS-CoV in HAE cultures. A dose-dependent reduction in replication approaching 1 $\log_{10}$ was observed at 0.1 μM and exceeded 2 $\log_{10}$ at 1 μM GS-5734 as compared to untreated controls (Fig. 2, A and B), with average IC_{50} values of 0.069 μM (SARS-CoV) and 0.074 μM (MERS-CoV). In parallel, we assessed the abundance of intracellular genomic [open reading frame 1a (ORF1a)] and subgenomic viral RNA [open reading frame nucleocapsid (ORFN)] via quantitative reverse transcription polymerase chain reaction (qRT-PCR). A dose-dependent reduction in both ORF1a and ORFN was observed for both SARS-CoV and MERS-CoV (Fig. 2, C and D, and table S1), consistent with titer reduction. The number of MERS-CoV–infected HAE cells also diminished with increasing dose of GS-5734, as observed by microscopy (Fig. 2E). To assess cytotoxicity of GS-5734 in HAE, we first measured the transcript levels of multiple proapoptotic and antiapoptotic factors within the signaling cascades of two different death receptors, TNF (tumor necrosis factor) and FAS (Fas cell surface death receptor) (fig. S2, A and B, and table S2). Unlike the positive control drug staurosporine, which uniformly up-regulated the transcription of all apoptosis factors measured, we did not observe a dose-dependent effect with GS-5734 treatment at concentrations that inhibit CoV replication. We then measured cytotoxicity via CellTiter-Glo assay in HAE treated with 10 or 0.1 μM GS-5734 or DMSO for 48 hours. As expected, GS-5734 treatment was similar to that of DMSO (CC_{50} in HAE > 10 μM; therapeutic index, >100; fig. S2C). To assess cytotoxicity of GS-5734 in an additional primary human lung cell type, we exposed normal human bronchiolar epithelial (NHBE) cell cultures to dilutions of GS-5734 or two known cytotoxic compounds, puromycin or staurosporine (fig. S3). In NHBE, the average CC_{50} for GS-5734 was determined to be 45 μM, which is 1800-fold above the observed IC_{50} value for MERS-CoV in 2B4 cells (0.025 μM) and 600-fold above the observed IC_{50} value for MERS-CoV in HAE cells (0.074 μM) (fig. S3, A and B). Together, we demonstrate antiviral efficacy in HAE against both SARS-CoV and MERS-CoV at concentrations that are at least 100-fold lower than those with observable cytotoxicity.

GS-5734 is effective against a diverse array of human and zoonotic CoV in HAE

CoV host specificity and entry into host cells are guided by the viral spike glycoprotein whose extensive genetic variation is a reflection of host species diversity and variation in virus receptor usage (Fig. 3A). Conversely, the CoV RdRp nsp12 is highly conserved between CoVs especially within genogroups (Fig. 3A), making it a potentially broadly applicable drug target.

Because we observed an antiviral effect against the two members of genogroup 2 (SARS-CoV and MERS-CoV), we sought to assess the breadth of antiviral activity against a genetically diverse array of human and zoonotic bat CoV in HAE cells. Treatment of HAE cultures with GS-5734 infected with human CoV NL63, a circulating group 1 human CoV that typically causes bronchitis (*12*), resulted in a pronounced 3 $\log_{10}$ reduction in virus production at 0.1 μM and undetectable virus at higher concentrations (Fig. 3B). Likewise, GS-5734 treatment inhibited replication of very diverse SARS-CoV–like group 2b (HKU3, WIV1, and SHC014) and MERS-CoV–like group 2c (HKU5) bat CoVs. Among these, WIV1 and SHC014 pose particular concern as "prepandemic strains," which can infect HAE cultures without adaptation and are thus poised for emergence in humans (*5*, *6*). With 1 μM GS-5734, infectious virus production of bat CoV was reduced by 1.5 $\log_{10}$ to 2 $\log_{10}$, and levels of viral genomes and subgenomic transcripts were reduced by 1 $\log_{10}$ to 2 $\log_{10}$ (Fig. 3B). Together, these data suggest that

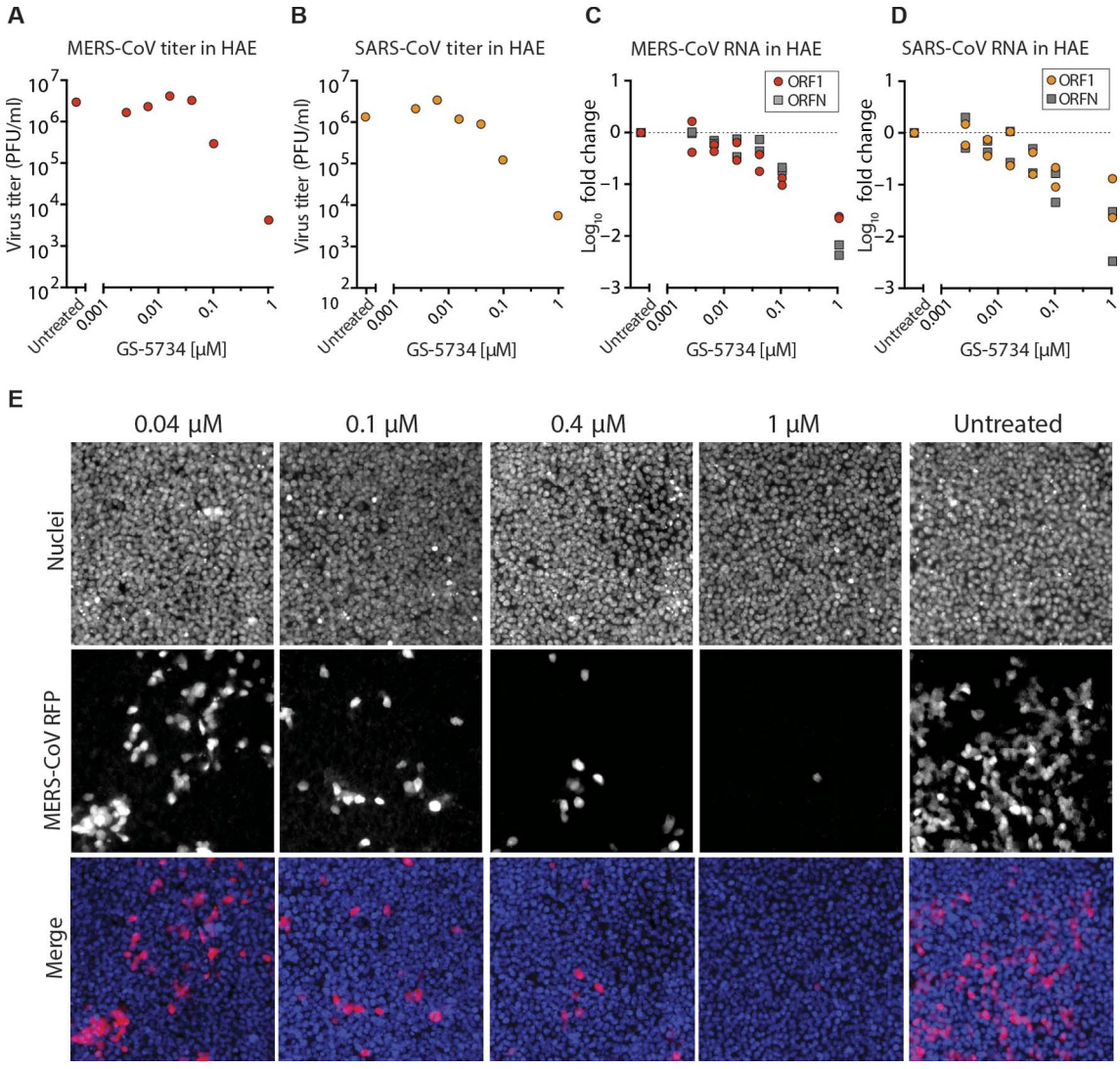

Fig. 2. GS-5734 prevents SARS-CoV and MERS-CoV replication in HAE cells. (**A**) Antiviral efficacy of GS-5734 against MERS-CoV in primary HAE cell cultures. HAE cells were infected with MERS-CoV red fluorescent protein (RFP) at an MOI of 0.5 in duplicate in the presence of GS-5734 for 48 hours, after which apical washes were collected for virus titration. Representative data from two separate experiments with three different cell donors are displayed. PFU, plaque-forming units. (**B**) Antiviral efficacy of GS-5734 against SARS-CoV in HAE cells. Cultures were infected with SARS-CoV green fluorescent protein (GFP), treated, and analyzed as described in (A). (**C**) qRT-PCR for MERS-CoV ORF1 and ORFN mRNA. Total RNA was isolated from cultures in (A) for qRT-PCR analysis. (**D**) qRT-PCR for SARS-CoV ORF1 and ORFN in cells from (C), as described in (B). (**E**) HAE cells were infected with MERS-CoV RFP and treated with GS-5734 as in (A). Nuclei were stained with Hoechst 33258 before fluorescent imaging.

GS-5734 can inhibit a broad range of diverse CoV including circulating human CoV, zoonotic bat CoV, and prepandemic zoonotic CoV.

Prophylactic treatment with GS-5734 reduces SARS-CoV disease

GS-5734 has relatively poor plasma stability in mice (that is, half-life, <5 min) due to expression of a secreted carboxylesterase 1c (*Ces1c*) absent in humans (*13*). Plasma stability of GS-5734 was markedly increased (half-life, ~25 min; fig. S4) in mice genetically deleted for *Ces1c* (*Ces1c*$^{-/-}$). We confirmed that SARS-CoV pathogenesis as measured by weight loss and lung viral titers was similar in wild-type (WT) C57BL/6J and *Ces1c*$^{-/-}$ mice through the infection of age- and sex-matched mice from both strains (fig. S4). We then assessed the pharmacokinetic (PK) profile in *Ces1c*$^{-/-}$ mice dosed subcutaneously with 50 mg/kg once daily (QD) or 25 mg/kg twice daily (BID). Plasma concentrations of prodrug diminished rapidly, accompanied by transient exposure to the alanine metabolite (Ala-Met) and more persistent exposure to the nucleoside analog (Fig. 4A). The plasma PK profile in esterase-deficient mice was similar to that reported previously in monkeys (*8*), but tissue accumulation of metabolites was ~10-fold less efficient in mice, suggesting that high doses and corresponding plasma exposures are necessary to obtain lung TP levels similar to those predicted in human. The metabolite profile in the lung showed the TP to be the dominant intracellular metabolite, establishing the less technically challenging assessment of total lung metabolite levels as a close approximation of TP (Fig. 4B). Although both 50 mg/kg QD and 25 mg/kg BID resulted in target maximal lung levels, tissue activation was not only less efficient in mouse but also the TP had a substantially shorter half-life in the mouse lung (~3 hours) relative to that observed in human lung cells in vitro or the nonhuman primate lung in vivo (half-life, ~20 hours; fig. S5). Therefore,

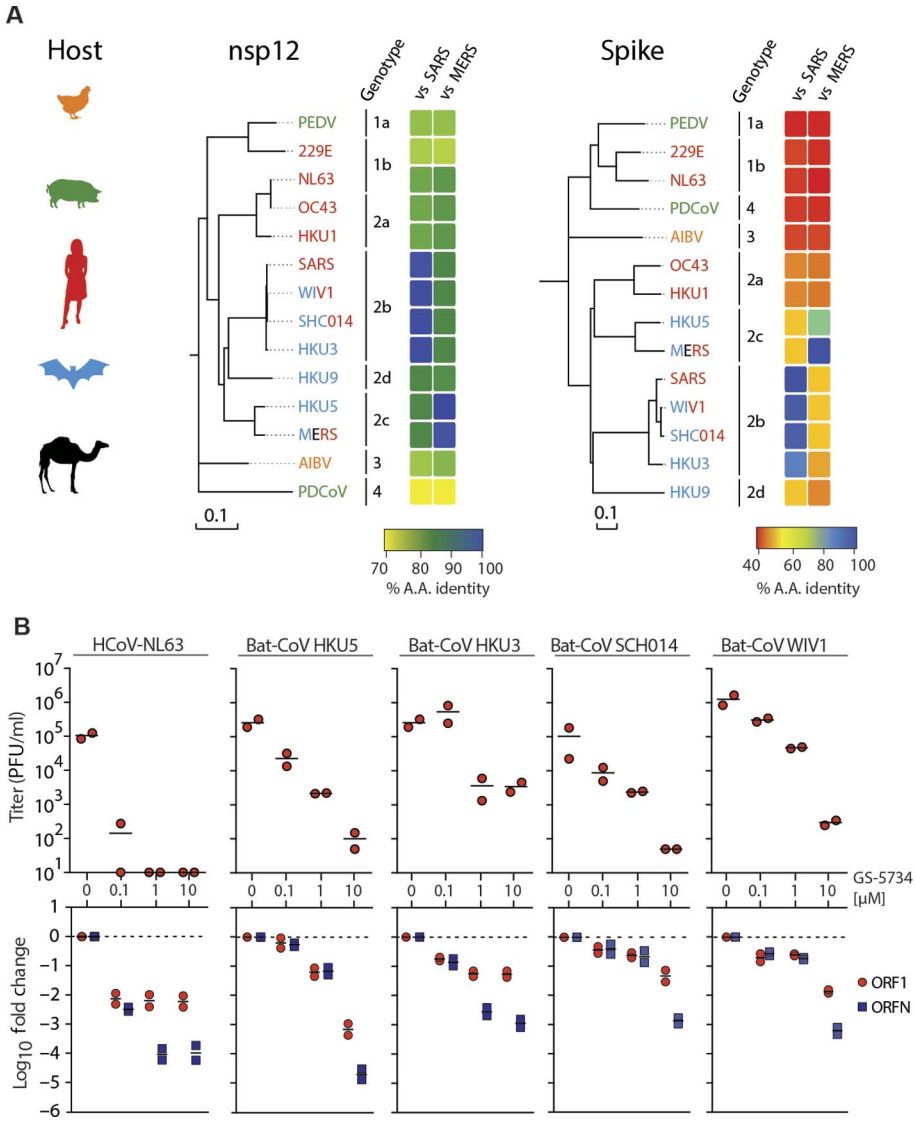

Fig. 3. GS-5734 is effective against a diverse array of human and zoonotic CoV in HAE. (**A**) Neighbor-joining trees created with representatives from all four CoV genogroups showing the genetic similarity of CoV nsp12 (RdRp) and CoV spike glycoprotein, which mediates host tropism and entry into cells. Text color of the virus strain label corresponds to virus host species on the left. The heatmap adjacent to each neighbor-joining tree depicts percent amino acid identity (% A.A. identity) against SARS-CoV or MERS-CoV. (**B**) Top: Antiviral efficacy of GS-5734 in HAE cells against circulating group 1 human CoV (HCoV-NL63) and bat CoV from group 2b (HKU3, SHC014, and WIV1) and 2c (HKU5). HAE cells were infected at an MOI of 0.5 in the presence of GS-5734 in duplicate. After 48 hours, virus produced was titrated via plaque assay. Each data point represents the titer per culture. Bottom: qRT-PCR for CoV ORF1 and ORFN mRNA in total RNA from cultures in the top panel.

only the BID-dosing regimen was able to maintain lung levels between 12 and 24 hours, consistent with those anticipated in humans and sufficient to maintain CoV inhibition over the dosing interval (Fig. 4C).

Mouse models of SARS-CoV disease faithfully recapitulate many aspects of SARS-CoV pathogenesis in humans including anorexia, high titers of virus replication in the lung, and the development of acute respiratory distress syndrome (ARDS) as well as an age-related exacerbation of disease (*14*). As shown in Fig. 5A, prophylactic administration at 50 mg/kg QD or 25 mg/kg BID ameliorated SARS-CoV–induced weight loss seen with vehicle treatment. Virus titers in the lung were significantly reduced ($P < 0.05$) on both 2 and 5 days post-infection (dpi) in GS-5734–treated mice as compared to vehicle-treated animals (Fig. 5B). In addition, levels of viral antigen staining in lung sections of GS-5734–treated animals were significantly lower ($P < 0.05$) as compared to vehicle-treated animals (Fig. 5, C and D). Treatment with GS-5734 also reduced SARS-CoV–induced lung pathology, including denuding bronchiolitis, perivascular accumulation of inflammatory infiltrates (that is, "cuffing"), and intra-alveolar edema associated with diffuse alveolar damage as compared to vehicle-treated animals (Fig. 5E and fig. S6).

Prophylactic treatment with GS-5734 prevented defects in pulmonary function seen in SARS-CoV–infected, vehicle-treated animals, as measured by whole-body plethysmography (WBP), an extremely sensitive means of quantitating pulmonary function (*15*). Penh, a surrogate measure of airway resistance or accumulation of debris in the airway, was significantly ($P < 0.05$) elevated in vehicle-treated animals as compared to those treated with GS-5734 (Fig. 5F). Metrics of labored breathing, such as increased exhalation time and extended pause in between the end of one breath and the beginning of the next, were increased in vehicle-treated animals as compared to those administered with GS-5734 (Fig. 5F).

Therapeutic postexposure administration of GS-5734 mitigates disease

Because prophylactic administration of GS-5734 reduced virus lung titers, improved lung function, and ameliorated symptoms of SARS-CoV disease, it was of interest to determine whether therapeutic treatment would also be effective. First, we compared the antiviral efficacy of GS-5734 (25 mg/kg, BID) beginning at −1 dpi (that is, prophylactic) or +1 dpi (that is, therapeutic). Therapeutic GS-5734 substantially reduced the SARS-CoV–induced weight loss in infected animals (Fig. 6, A and B) and significantly suppressed virus lung titers ($P = 0.0059$), thus demonstrating that therapeutic administration of GS-5734 can reduce disease and suppress replication during an ongoing infection (Fig. 6C). Therapeutic treatment significantly ($P = 0.003$) improved pulmonary function (that is, reduced Penh scores) as compared to vehicle-treated controls (Fig. 6D). We then explored the therapeutic potential of GS-5734 given at 2 dpi, which is after virus replication and lung airway epithelial damage have peaked (fig. S7). Disease severity and survival did not differ with treatment, but we observed a significant reduction ($P < 0.05$) in SARS-CoV lung titers of GS-5734–treated animals at 6 dpi. These data suggest that reductions in viral load after peak lung titers were achieved were insufficient to improve outcomes after the immunopathological phase of disease had been initiated. Thus, in the mouse, if given before the peak of SARS-CoV replication and peak damage to the airway epithelium,

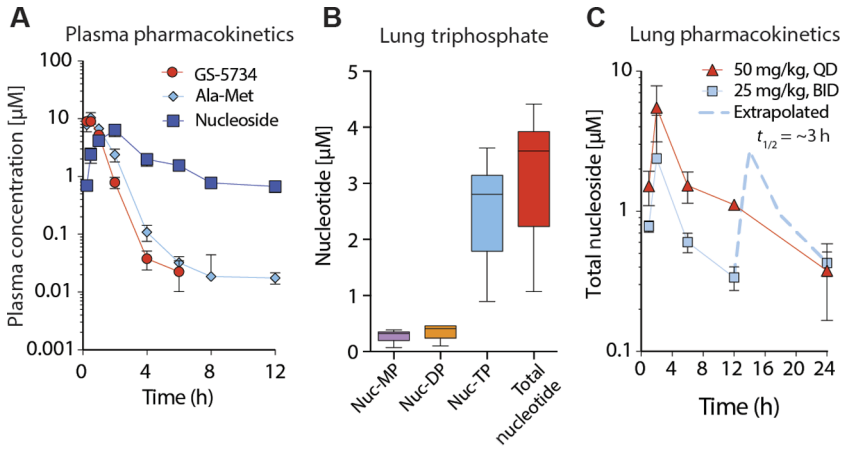

Fig. 4. Pharmacokinetics of GS-5734 in *Ces1c*$^{-/-}$ mice. (**A**) Pharmacokinetics in *Ces1c*$^{-/-}$ mouse plasma after subcutaneous administration of GS-5734 (25 mg/kg). Longitudinal plasma samples were taken to measure prodrug GS-5734, intermediate metabolites Ala-Met, and nucleoside by LC-MS. (**B**) Lung TP in *Ces1c*$^{-/-}$ mouse lung 4 hours after subcutaneous administration of GS-5734 (50 mg/kg). Nucleotide monophosphate (Nuc-MP), diphosphate (Nuc-DP), triphosphate (Nuc-TP), and total nucleotide (sum of Nuc-MP, Nuc-DP, and Nuc-TP) are displayed. (**C**) Pharmacokinetics of total nucleotide in *Ces1c*$^{-/-}$ mouse lung after subcutaneous administration of GS-5734 at 25 mg/kg BID or 50 mg/kg QD.

GS-5734 can improve pulmonary function, reduce viral loads, and diminish disease.

DISCUSSION

Emerging viral infections represent a critical global health concern because specific antiviral therapies and vaccines are usually lacking. To maximize the potential public health benefit of therapeutics against emerging viruses, they should be efficacious against past (that is, SARS-CoV), current (that is, MERS-CoV), and future emerging viral threats. Knowledge of the spectrum of therapeutic efficacy is essential for making informed clinical decisions, especially in the early stages of an outbreak. Because zoonotic CoV emergence is driven by an amalgamation of human, wild animal, and viral factors, it is difficult to gauge zoonotic CoV emergence potential based on viral genome sequences alone (*2*). Here, we provide an example of a successful public-private partnership that combines metagenomics, synthetic biology, primary human cell culture models, drug metabolism, PKs, and in vivo models of viral pathogenesis to demonstrate broad-spectrum activity of a drug candidate against a virus family prone to emergence (fig. S8). Although we demonstrated broad-spectrum efficacy against human and zoonotic CoV from multiple CoV genogroups, we have not yet assessed antiviral efficacy for all CoV genogroups, which is a limitation of our current study. Nevertheless, our panel of reconstructed human and zoonotic bat CoV was essential to determine whether GS-5734 would be efficacious against highly divergent emerged (SARS-CoV), emerging (MERS-CoV), and circulating zoonotic strains with pandemic potential (that is, WIV1 and SHC014) (*5*, *6*, *16*, *17*). In the future, the rapid development of vaccines, therapies, and diagnostics for emerging viruses will be dependent on the reconstruction and the in vitro and in vivo adaptation of these viruses in the laboratory.

Here, we report the broad-spectrum antiviral efficacy of a small molecule against multiple genetically distinct CoV in vitro and in vivo. Current vaccine and human monoclonal antibody approaches have proven to be effective but typically have limited breadth of protection due to antigenic diversity in the CoV spike glycoprotein (*5*, *6*). Conversely, RdRp-targeting therapies such as GS-5734 are more likely to be broadly active against past, current, and future CoV due to the inherent genetic conservation of the CoV replicase. As evidenced by the failure of the nucleoside prodrug balapiravir to translate in vitro efficacy into in vivo efficacy in mice and humans, antiviral drug candidates should be thoroughly evaluated in the most biologically relevant models of pathogenesis to maximize clinical translatability (*18*). Cell type–specific differences in the active transport and/or metabolism of nucleoside analogs may affect the antiviral profile (*19*). Thus, we aimed to expand on previous in vitro studies of SARS-CoV and MERS-CoV antiviral efficacy that were limited to monkey kidney cancer cell lines (*8*, *9*). Similar in cellular complexity and physiology to the human conducting airway, the HAE cell culture contains mucus-secreting cells, basolateral cells, and some of the main target cells of SARS-CoV (ciliated epithelial cells) and MERS-CoV (nonciliated epithelial cells) in vivo (*11*, *20*). With our HAE cell antiviral efficacy data, we provide strong evidence that GS-5734 will be taken up and metabolized in cells targeted by multiple human and zoonotic CoV in the human lung.

Preclinical in vivo antiviral efficacy studies provide insight into the PK/pharmacodynamic (PD) relationship of a drug from which effective dosing regimens can be extrapolated for human clinical trial. To maximize the utility of preclinical PK/PD studies, the use of animal models that accurately recapitulate human disease is essential. Multiple aspects of the human disease are captured by the mouse-adapted SARS-CoV (SARS-CoV MA15) model used herein, including high-titer virus replication limited to the lung, the development of ARDS, age-related exacerbation of disease, and death. In contrast to humans infected with SARS-CoV where viral titers peak 7 to 10 days after the onset of symptoms, virus titers in the lungs of SARS-CoV MA15–infected C57BL/6 mice rapidly increase 4 to 5 logs and peak at 2 dpi, concurrent with maximal damage to the conducting airway epithelium and alveoli (*14*). After 2 dpi, virus titers wane, and the remainder of the disease course is driven by immunopathology. Thus, the 7 to 10 days before peak replication in humans is compressed into the first 48 hours of our mouse model. Similar to humans, disease severity in SARS-CoV–infected mice is directly correlated with lung viral load, which can be modulated through increasing dose of input virus (*14*, *21*). With both prophylactic (−1 dpi) and therapeutic (+1 dpi) dosing of GS-5734, we demonstrate a reduction in replication below a disease-causing threshold. Therapeutic treatment beginning at 2 dpi reduced lung viral loads yet did not improve disease outcomes, suggesting that antivirals initiated after virus replication and immunopathology have reached their tipping point were not clinically beneficial. This result is not surprising given the precedent set by the influenza antiviral oseltamivir, where treatment efficacy diminishes with time after the onset of symptoms (*22*). Like SARS-CoV, MERS-CoV titers in the respiratory tract peak in the second week after the onset of symptoms (*23*). Thus, the window in which to administer antiviral treatment after the onset of symptoms but before achieving peak virus titers should be prolonged in humans as compared to experimentally infected mice. Unfortunately, the differences in SARS-CoV pathogenesis among mice and humans noted above limit our ability to determine the time at which treatment no longer will provide a clinical benefit in humans. Nevertheless, our studies provide data that strongly support the testing of GS-5734 in nonhuman primates and suggest that therapeutic treatment of MERS-CoV–infected

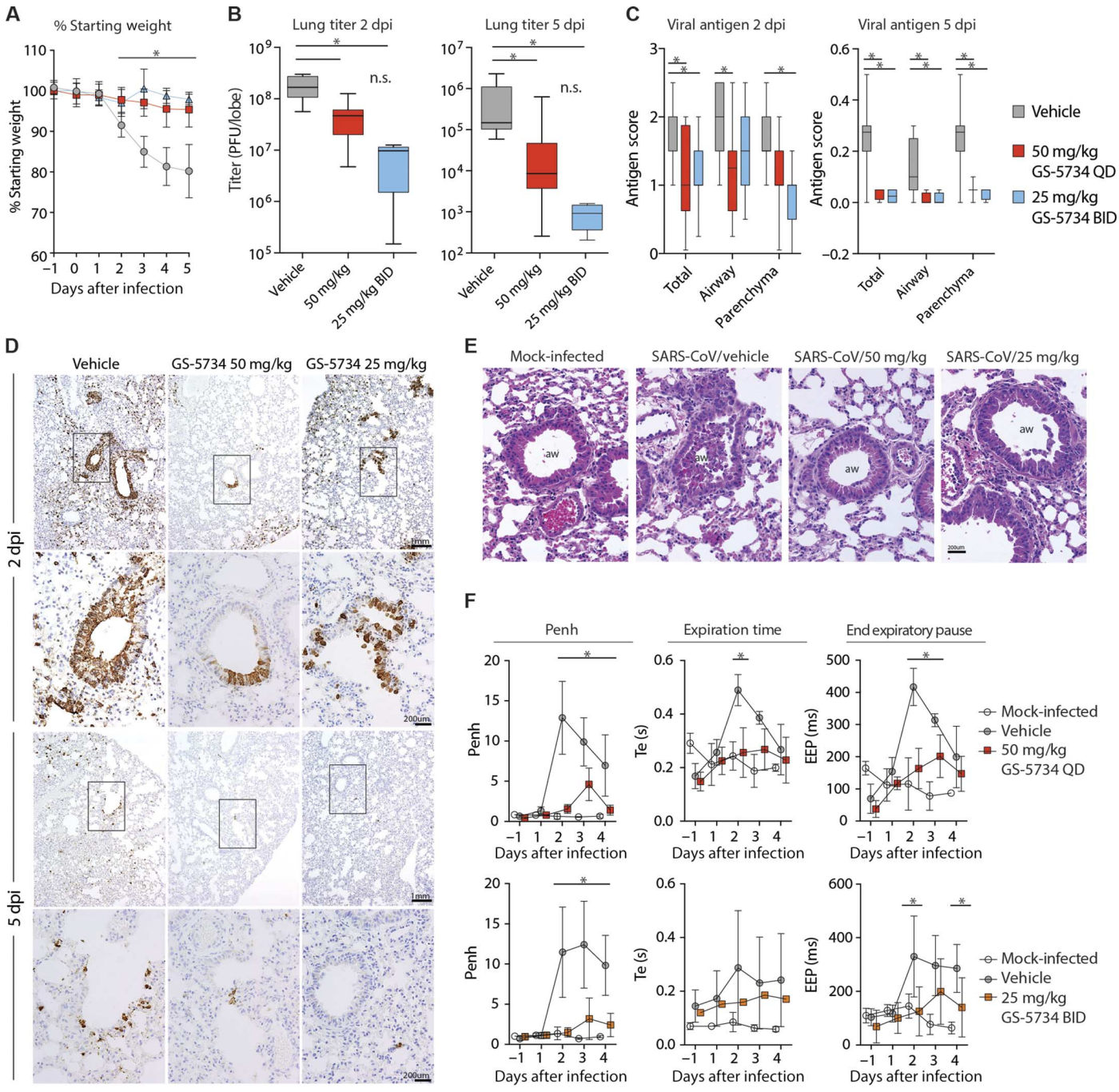

Fig. 5. Prophylactic treatment with GS-5734 reduces SARS-CoV disease. (**A**) Percent starting weight of *Ces1c*$^{-/-}$ mice infected with 10^4 PFU SARS-CoV MA15 treated beginning at −1 dpi with either vehicle (n = 42) or GS-5734 [25 mg/kg BID (n = 25) or 50 mg/kg QD (n = 28)]. (**B**) SARS-CoV lung titer of mice in (A) at 2 dpi (vehicle, n = 11; 50 mg/kg, n = 11; 25 mg/kg, n = 5) (left) or 5 dpi (vehicle, n = 13; 50 mg/kg, n = 13; 25 mg/kg, n = 4) (right). n.s., not significant. (**C**) Quantitation of SARS-CoV antigen in lung sections of mice in (A) at 2 dpi (left) (vehicle, n = 15; 50 mg/kg, n = 12; 25 mg/kg, n = 7) (left) or 5 dpi (vehicle, n = 10; 50 mg/kg, n = 12; 25 mg/kg, n = 4) (right). (**D**) Photomicrographs of SARS-CoV antigen staining (brown) and nuclei (blue) in lung sections from 2 and 5 dpi. (**E**) Photomicrographs of hematoxylin and eosin–stained mouse lung sections from 2 dpi highlighting the conducting airway lumen (aw). (**F**) WBP was used to measure the pulmonary function of mice in (A). Penh is a surrogate measure of bronchoconstriction. Expiration time (t_e) is the time taken to release one breath. End of expiratory pause (EEP) is the time between breaths. Symbols and error bars for (A), (B), (D), and (I) represent the mean and SD. The boxes encompass the 25th to 75th percentile, whereas the whiskers represent the range in (C), (E), and (F). Asterisk indicates statistical significance ($P < 0.05$) by two-way analysis of variance (ANOVA) with Tukey's multiple comparison test for (D), (F), and (I) and with Kruskal-Wallis test for (E).

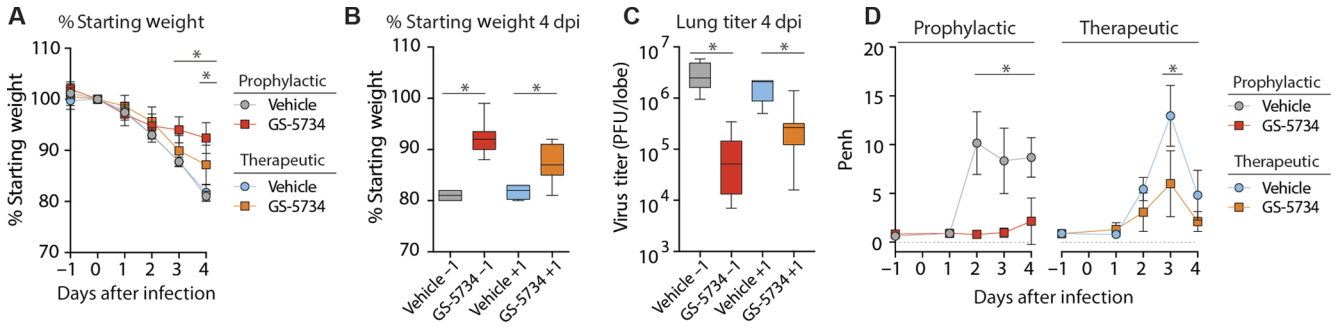

Fig. 6. Therapeutic postexposure administration of GS-5734 mitigates disease. (**A**) Percent starting weight of 27- to 28-week-old female *Ces1c*$^{-/-}$ mice infected with 10^3 PFU SARS-CoV MA15 and treated BID with vehicle or GS-5734 (25 mg/kg) beginning on either −1 dpi (vehicle, $n = 5$; GS-5734, $n = 10$) or +1 dpi (vehicle, $n = 4$; GS-5734, $n = 11$). Weights of GS-5734–treated animals were statistically different ($P < 0.05$) from those of vehicle-treated animals at 3 and 4 dpi for prophylactic groups and at 4 dpi for therapeutic groups by two-way ANOVA with Tukey's multiple comparison test. (**B**) Percent starting weights of mice in (A) at 4 dpi. (**C**) SARS-CoV lung titer in mice infected and treated as described in (A). Asterisks indicate statistical significance ($P < 0.05$) by Mann-Whitney test for (B) and (C). (**D**) WBP was used to measure the pulmonary function in mice infected and treated as described in (A). Penh is a surrogate measure of bronchoconstriction or airway obstruction. Asterisks indicate statistical significance by two-way ANOVA with Šidák's multiple comparison test.

humans with GS-5734 will help diminish virus replication and disease if administered early enough during the course of infection.

Currently, there are no approved antiviral treatments for SARS-CoV or MERS-CoV that specifically target the virus. Multiple therapeutic approaches against SARS-CoV and MERS-CoV are currently in development including immunomodulation, vaccination, DAAs, and host-targeted antivirals (*7*). Known antivirals, such as ribavirin and lopinavir-ritonavir, and immunomodulators, such as interferon and corticosteroids, have been used to treat both SARS-CoV and MERS-CoV patients, but none were proven effective in randomized controlled trials (*7*). Cell culture studies in multiple cell lines have demonstrated antiviral effects of several U.S. Food and Drug Administration–approved drugs (ritonavir, lopinavir, nelfinavir, mycophenolic acid, and ribavirin), but contradictory results and experimental incongruities make the interpretation difficult (*24*–*29*). Small molecules targeting SARS-CoV and MERS-CoV have been assessed in cancer cell lines in vitro, but their antiviral efficacy against other human or zoonotic CoV remains unknown (*16*, *30*). Very few small molecules have been assessed in CoV animal models of viral pathogenesis, and some have even been shown to exacerbate disease (for example, ribavirin and mycophenolic acid) (*31*, *32*). Although the *Ces1c*$^{-/-}$ mice used herein foster increased drug stability, they are not suitable for MERS-CoV efficacy studies because the murine ortholog of the MERS-CoV receptor, dipeptidyl peptidase 4 (DPP4), does not facilitate MERS-CoV infection (*33*). Thus, our in vivo studies were limited to SARS-CoV, and future studies assessing MERS-CoV efficacy in double-transgenic humanized DPP4/*Ces1c*$^{-/-}$ mice are planned. Human safety testing for GS-5734 is ongoing, and the drug has already been used to treat a small number of Ebola virus–infected patients under the "compassionate use" clause (*34*). Overall, our work provides evidence that GS-5734 may protect CoV-infected patients from progression to severe disease and could prophylactically protect health care workers in areas with existing endemic MERS-CoV and that its broad-spectrum activity may prove valuable when a novel CoV emerges in the future.

MATERIALS AND METHODS

Study design

The primary goal of this study was to determine whether the small-molecule nucleoside analog GS-5734 exhibited broad-spectrum antiviral activity against the CoV family. Using multiple in vitro models including human primary cells, we measured the antiviral effect of GS-5734 on multiple CoV, encompassing much of the inherent family-wide genetic diversity. Data presented for studies in human primary cultures are representative of those from three human donors. Cytotoxicity was assessed in the 2B4 cell line and in two human primary lung cell types. Experiments were performed in triplicate unless otherwise stated. Drug effects were measured relative to vehicle controls. The secondary goal of this study was to assess antiviral efficacy in vivo within mouse models of severe CoV disease. The in vivo efficacy studies were intended to gain the data required to justify further testing in nonhuman primates and collectively inform future human clinical trials. Mice were age- and sex-matched and randomly assigned into groups before infection and treatment. The prophylactic and therapeutic in vivo studies presented in the main text were repeated at least once. Pathology and SARS-CoV antigen scoring were performed in a blinded manner. Exclusion criteria for in vivo studies were as follows: If a given mouse unexpectedly did not lose weight after infection and their virus lung titers were more than 2 $\log_{10}$ lower the mean of the group, this indicated that infection was inefficient and all data related to that mouse were censored. Primary data are located in table S3.

Viruses

SARS-CoV expressing GFP (GFP replaces ORF7) and MERS-CoV expressing RFP (RFP replaces ORF3) were created from molecular complementary DNA clones as described (*11*, *20*). To create SARS-CoV and MERS-CoV expressing nLUC, the genes for GFP and RFP were replaced with nLUC and isolated as referenced above. Recombinant human CoV NL63 and recombinant bat CoV for strains HKU3, HKU5, WIV1, and SHC014 were created as described (*5*, *6*, *12*, *16*, *17*).

GS-5734

GS-5734 was synthesized at Gilead Sciences Inc., and its chemical identity and purity were determined by nuclear magnetic resonance, high-resolution mass spectrometry, and high-performance liquid chromatography (HPLC) analysis (*9*). GS-5734 was solubilized in 100% DMSO for in vitro studies and in vehicle containing 12% sulfobutylether-β-cyclodextrin in water (with HCl/NaOH) at pH 5 for in vivo studies. GS-5734 was made available to the University of North Carolina (UNC) at Chapel Hill under a materials transfer agreement with Gilead Sciences.

In vitro efficacy and cytotoxicity in 2B4 cells

The human lung epithelial cell line 2B4 was maintained in Dulbecco's modified Eagle's medium (Gibco), 20% fetal bovine serum (HyClone), and 1× antibiotic-antimycotic (Gibco) (*10*). Twenty-four hours after plating 5×10^4 cells per well, fresh medium was added. In triplicate, cells were infected for 1 hour with MERS-nLUC diluted in growth medium (MOI of 0.08), after which virus was removed, cultures were rinsed once, and fresh medium containing dilutions of GS-5734 or vehicle was added. DMSO (0.05%) was constant in all conditions. At 48 hours postinfection (hpi), virus replication was measured by nLUC assay (Promega), and cytotoxicity was measured via CellTiter-Glo (Promega) assay and then read on a SpectraMax plate reader (Molecular Devices). The IC_{50} value was defined in GraphPad Prism 7 (GraphPad) as the concentration at which there was a 50% decrease in viral replication using ultraviolet-treated MERS-nLUC (100% inhibition) and vehicle alone (0% inhibition) as controls. CC_{50} value was determined through comparison of data with that from cell-free (100% cytotoxic) and vehicle-only (0% cytotoxic) samples.

In vitro efficacy and toxicity in HAE cells

HAE cell cultures were obtained from the Tissue Procurement and Cell Culture Core Laboratory in the Marsico Lung Institute/Cystic Fibrosis Research Center at UNC. Before infection, HAE were washed with phosphate-buffered saline (PBS) and moved into air-liquid interface medium containing various doses of GS-5734 ranging from 10 to 0.00260 μM (final DMSO, <0.05%) (*11*). HAE cultures were infected at an MOI of 0.5 for 3 hours at 37°C, after which virus was removed, and cultures were washed with PBS and then incubated at 37°C for 48 hours. Fluorescent images of MERS-RFP were taken at 48 hpi after nuclear staining with Hoechst 33258. Virus replication/titration was performed as previously described (*11*). Similar data were obtained using cells from three different patient donors. Cytotoxicity was measured via CellTiter-Glo (Promega) in duplicate HAE cell cultures treated with 10 or 0.1 μM GS-5734 or DMSO at 0.05%.

In vivo pharmacokinetic analysis in plasma after GS-5734 administration in *Ces1c*$^{-/-}$ mice and marmosets

Mice were subcutaneously administered with GS-5734 (25 mg/kg), after which plasma was isolated from triplicate mice at 0.25, 0.5, 1, 2, 4, 6, 8, and 12 hours after administration. Three male marmosets were administered a single dose of GS-5734 intravenously at 10 mg/kg, after which plasma was isolated at 0.083, 0.25, 0.5, 1, 2, 4, 8, and 24 hours after administration. For both mouse and marmoset, 25 μl of plasma was treated and analyzed as described in the Supplementary Materials and Methods "Stability of GS-5734 in WT or *Ces1c*$^{-/-}$ mouse plasma." Plasma concentrations of GS-5734, alanine metabolite (Ala-Met), and nucleoside monophosphate were determined using 8- to 10-point calibration curves spanning at least three orders of magnitude with quality control samples to ensure accuracy and precision and prepared in normal mouse plasma. Analytes were separated by a 75 × 2 mm (4-μm) Synergi Hydro-RP 30A column (Phenomenex) using a multistage linear gradient from 0.2 to 99% acetonitrile in mobile phase A at a flow rate of 260 μl/min.

Quantitation of GS-5734 metabolites in the lung after GS-5734 administration in *Ces1c*$^{-/-}$ mice and marmosets

Mice were dosed with GS-5734 (25 or 50 mg/kg), as described above. Lungs from triplicate mice were isolated at 1, 2, 6, 12, and 24 hours after administration and snap-frozen. Four male marmosets were dosed with GS-5734, as described above, and lungs were isolated at 2 and 24 hours after administration and were snap-frozen. On dry ice, frozen lung samples were pulverized and weighed. Dry ice–cold extraction buffer containing 0.1% potassium hydroxide and 67 mM EDTA in 70% methanol and containing 0.5 μM chloroadenosine triphosphate as internal standard was added and homogenized. After clarifying centrifugation at 20,000*g* for 20 min, supernatants were dried in a centrifuge evaporator. Dried samples were then reconstituted with 60 μl of mobile phase A, containing 3 mM ammonium formate (pH 5) with 10 mM dimethylhexylamine in water, and centrifuged at 20,000*g* for 20 min, with final supernatants transferred to HPLC injection vials. An aliquot of 10 μl was subsequently injected onto an API 5000 LC/MS/MS system for analysis performed using a similar method, as described for intracellular metabolism studies.

Prophylactic and therapeutic efficacy of GS-5734 against SARS-CoV in *Ces1c*$^{-/-}$ mice

Male and female (25- to 28-week-old) mice genetically deleted for carboxylesterase 1C (*Ces1c*$^{-/-}$) (stock 014096, The Jackson Laboratory) were anesthetized with ketamine/xylazine and infected with 10^4 PFU/50 μl (prophylactic studies) or 10^3 PFU/50 μl (therapeutic studies) SARS-CoV MA15. Animals were weighed daily to monitor virus-associated weight loss and to determine the appropriate dose volume of GS-5734 or vehicle. GS-5734 or vehicle was administered subcutaneously BID, 12 hours apart. On 2 and 5 dpi (prophylactic) or 2 and 4 or 6 dpi (therapeutic), animals were sacrificed by isoflurane overdose, and the large left lobe was frozen at −80°C for viral titration via plaque assay, as described (*14*). The inferior right lobe was placed in 10% buffered formalin and stored at 4°C until histological analysis. Aberrations in lung function were determined by WBP (Data Sciences International), as described (*15*).

Biocontainment and biosafety

Reported studies were initiated after the UNC Institutional Biosafety Committee approved the experimental protocols under the Baric Laboratory Safety Plan (20167715). SARS-CoV is a select agent. All work for these studies was performed with approved standard operating procedures for SARS-CoV, MERS-CoV, and other related CoVs in facilities conforming to the requirements recommended in the Biosafety in Microbiological and Biomedical Laboratories, the U.S. Department of Health and Human Services, the U.S. Public Health Service, the U.S. Centers for Disease Control and Prevention, and the National Institutes of Health.

Animal care

Efficacy studies were performed in animal biosafety level 3 facilities at UNC Chapel Hill. All works were conducted under protocols approved by the Institutional Animal Care and Use Committee at UNC Chapel Hill (protocol #13-288; continued on #16-284) according to guidelines set by the Association for the Assessment and Accreditation of Laboratory Animal Care and the U.S. Department of Agriculture.

Statistics

All statistical calculations were performed in GraphPad Prism 7. Specific tests to determine statistical significance are noted in each figure legend.

SUPPLEMENTARY MATERIALS

www.sciencetranslationalmedicine.org/cgi/content/full/9/396/eaal3653/DC1

Materials and Methods

Fig. S1. In vitro toxicity and efficacy of GS-5734 in 2B4 cells.

Fig. S2. In vitro toxicity of GS-5734 in primary HAE cell cultures.

Fig. S3. In vitro toxicity of GS-5734 in primary NHBE cell cultures.
Fig. S4. SARS-CoV in vivo pathogenesis is similar in WT and *Ces1c*$^{-/-}$ mice.
Fig. S5. Metabolism in NHBE cells and pharmacokinetic analysis in nonhuman primates.
Fig. S6. GS-5734 diminishes SARS-CoV–induced lung pathology.
Fig. S7. Therapeutic administration of GS-5734 beginning at 2 dpi does not provide a therapeutic benefit.
Fig. S8. A comprehensive platform approach to evaluate therapeutics against emerging viral infections.
Table S1. CoV genomic and subgenomic real-time primer sets.
Table S2. Primer/probe sets for indicators of cellular apoptosis/toxicity qRT-PCR.
Table S3. Primary data.

REFERENCES AND NOTES

1. L. D. Eckerle, M. M. Becker, R. A. Halpin, K. Li, E. Venter, X. Lu, S. Scherbakova, R. L. Graham, R. S. Baric, T. B. Stockwell, D. J. Spiro, M. R. Denison, Infidelity of SARS-CoV Nsp14-exonuclease mutant virus replication is revealed by complete genome sequencing. *PLOS Pathog.* **6**, e1000896 (2010).
2. E. de Wit, N. van Doremalen, D. Falzarano, V. J. Munster, SARS and MERS: Recent insights into emerging coronaviruses. *Nat. Rev. Microbiol.* **14**, 523–534 (2016).
3. A. Liljander, B. Meyer, J. Jores, M. A. Müller, E. Lattwein, I. Njeru, B. Bett, C. Drosten, V. M. Corman, MERS-CoV antibodies in humans, Africa, 2013–2014. *Emerg. Infect. Dis.* **22**, 1086–1089 (2016).
4. M. A. Müller, B. Meyer, V. M. Corman, M. Al-Masri, A. Turkestani, D. Ritz, A. Sieberg, S. Aldabbagh, B.-J. Bosch, E. Lattwein, R. F. Alhakeem, A. M. Assiri, A. M. Albarrak, A. M. Al-Shangiti, J. A. Al-Tawfiq, P. Wikramaratna, A. A. Alrabeeah, C. Drosten, Z. A. Memish, Presence of Middle East respiratory syndrome coronavirus antibodies in Saudi Arabia: A nationwide, cross-sectional, serological study. *Lancet Infect. Dis.* **15**, 559–564 (2015).
5. V. D. Menachery, B. L. Yount Jr., K. Debbink, S. Agnihothram, L. E. Gralinski, J. A. Plante, R. L. Graham, T. Scobey, X.-Y. Ge, E. F. Donaldson, S. H. Randell, A. Lanzavecchia, W. A. Marasco, Z.-L. Shi, R. S. Baric, A SARS-like cluster of circulating bat coronaviruses shows potential for human emergence. *Nat. Med.* **21**, 1508–1513 (2015).
6. V. D. Menachery, B. L. Yount Jr., A. C. Sims, K. Debbink, S. S. Agnihothram, L. E. Gralinski, R. L. Graham, T. Scobey, J. A. Plante, S. R. Royal, J. Swanstrom, T. P. Sheahan, R. J. Pickles, D. Corti, S. H. Randell, A. Lanzavecchia, W. A. Marasco, R. S. Baric, SARS-like WIV1-CoV poised for human emergence. *Proc. Natl. Acad. Sci. U.S.A.* **113**, 3048–3053 (2016).
7. A. Zumla, J. F. W. Chan, E. I. Azhar, D. S. Hui, K. Y. Yuen, Coronaviruses—Drug discovery and therapeutic options. *Nat. Rev. Drug Discov.* **15**, 327–347 (2016).
8. T. K. Warren, R. Jordan, M. K. Lo, A. S. Ray, R. L. Mackman, V. Soloveva, D. Siegel, M. Perron, R. Bannister, H. C. Hui, N. Larson, R. Strickley, J. Wells, K. S. Stuthman, S. A. Van Tongeren, N. L. Garza, G. Donnelly, A. C. Shurtleff, C. J. Retterer, D. Gharaibeh, R. Zamani, T. Kenny, B. P. Eaton, E. Grimes, L. S. Welch, L. Gomba, C. L. Wilhelmsen, D. K. Nichols, J. E. Nuss, E. R. Nagle, J. R. Kugelman, G. Palacios, E. Doerffler, S. Neville, E. Carra, M. O. Clarke, L. Zhang, W. Lew, B. Ross, Q. Wang, K. Chun, L. Wolfe, D. Babusis, Y. Park, K. M. Stray, I. Trancheva, J. Y. Feng, O. Barauskas, Y. Xu, P. Wong, M. R. Braun, M. Flint, L. K. McMullan, S. S. Chen, R. Fearns, S. Swaminathan, D. L. Mayers, C. F. Spiropoulou, W. A. Lee, S. T. Nichol, T. Cihlar, S. Bavari, Therapeutic efficacy of the small molecule GS-5734 against Ebola virus in rhesus monkeys. *Nature* **531**, 381–385 (2016).
9. A. Cho, O. L. Saunders, T. Butler, L. Zhang, J. Xu, J. E. Vela, J. Y. Feng, A. S. Ray, C. U. Kim, Synthesis and antiviral activity of a series of 1′-substituted 4-aza-7,9-dideazaadenosine C-nucleosides. *Bioorg. Med. Chem. Lett.* **22**, 2705–2707 (2012).
10. A. C. Sims, S. C. Tilton, V. D. Menachery, L. E. Gralinski, A. Schäfer, M. M. Matzke, B.-J. Webb-Robertson, J. Chang, M. L. Luna, C. E. Long, A. K. Shukla, A. R. Bankhead III, S. E. Burkett, G. Zornetzer, C.-T. K. Tseng, T. O. Metz, R. Pickles, S. McWeeney, R. D. Smith, M. G. Katze, K. M. Waters, R. S. Baric, Release of severe acute respiratory syndrome coronavirus nuclear import block enhances host transcription in human lung cells. *J. Virol.* **87**, 3885–3902 (2013).
11. A. C. Sims, R. S. Baric, B. Yount, S. E. Burkett, P. L. Collins, R. J. Pickles, Severe acute respiratory syndrome coronavirus infection of human ciliated airway epithelia: Role of ciliated cells in viral spread in the conducting airways of the lungs. *J. Virol.* **79**, 15511–15524 (2005).
12. E. F. Donaldson, B. Yount, A. C. Sims, S. Burkett, R. J. Pickles, R. S. Baric, Systematic assembly of a full-length infectious clone of human coronavirus NL63. *J. Virol.* **82**, 11948–11957 (2008).
13. B. Li, M. Sedlacek, I. Manoharan, R. Boopathy, E. G. Duysen, P. Masson, O. Lockridge, Butyrylcholinesterase, paraoxonase, and albumin esterase, but not carboxylesterase, are present in human plasma. *Biochem. Pharmacol.* **70**, 1673–1684 (2005).
14. L. E. Gralinski, A. Bankhead III, S. Jeng, V. D. Menachery, S. Proll, S. E. Belisle, M. Matzke, B.-J. Webb-Robertson, M. L. Luna, A. K. Shukla, M. T. Ferris, M. Bolles, J. Chang, L. Aicher, K. M. Waters, R. D. Smith, T. O. Metz, G. L. Law, M. G. Katze, S. McWeeney, R. S. Baric, Mechanisms of severe acute respiratory syndrome coronavirus-induced acute lung injury. *MBio* **4**, e00271–13 (2013).
15. V. D. Menachery, L. E. Gralinski, R. S. Baric, M. T. Ferris, New metrics for evaluating viral respiratory pathogenesis. *PLOS ONE* **10**, e0131451 (2015).
16. S. Agnihothram, B. L. Yount Jr., E. F. Donaldson, J. Huynh, V. D. Menachery, L. E. Gralinski, R. L. Graham, M. M. Becker, S. Tomar, T. D. Scobey, H. L. Osswald, A. Whitmore, R. Gopal, A. K. Ghosh, A. Mesecar, M. Zambon, M. Heise, M. R. Denison, R. S. Baric, A mouse model for *Betacoronavirus* subgroup 2c using a bat coronavirus strain HKU5 variant. *MBio* **5**, e00047–00014 (2014).
17. M. M. Becker, R. L. Graham, E. F. Donaldson, B. Rockx, A. C. Sims, T. Sheahan, R. J. Pickles, D. Corti, R. E. Johnston, R. S. Baric, M. R. Denison, Synthetic recombinant bat SARS-like coronavirus is infectious in cultured cells and in mice. *Proc. Natl. Acad. Sci. U.S.A.* **105**, 19944–19949 (2008).
18. N. M. Nguyen, C. N. B. Tran, L. K. Phung, K. T. H. Duong, A. Huynh Hle, J. Farrar, Q. T. H. Nguyen, H. T. Tran, C. V. Nguyen, L. Merson, L. T. Hoang, M. L. Hibberd, P. P. K. Aw, A. Wilm, N. Nagarajan, D. T. Nguyen, M. P. Pham, T. T. Nguyen, H. Javanbakht, K. Klumpp, J. Hammond, R. Petric, M. Wolbers, C. T. Nguyen, C. P. Simmons, A randomized, double-blind placebo controlled trial of balapiravir, a polymerase inhibitor, in adult dengue patients. *J. Infect. Dis.* **207**, 1442–1450 (2013).
19. K. D. Ibarra, J. K. Pfeiffer, Reduced ribavirin antiviral efficacy via nucleoside transporter-mediated drug resistance. *J. Virol.* **83**, 4538–4547 (2009).
20. T. Scobey, B. L. Yount, A. C. Sims, E. F. Donaldson, S. S. Agnihothram, V. D. Menachery, R. L. Graham, J. Swanstrom, P. F. Bove, J. D. Kim, S. Grego, S. H. Randell, R. S. Baric, Reverse genetics with a full-length infectious cDNA of the Middle East respiratory syndrome coronavirus. *Proc. Natl. Acad. Sci. U.S.A.* **110**, 16157–16162 (2013).
21. J. S. Peiris, C. M. Chu, V. C. C. Cheng, K. S. Chan, I. F. N. Hung, L. L. M. Poon, K. I. Law, B. S. F. Tang, T. Y. W. Hon, C. S. Chan, K. H. Chan, J. S. C. Ng, B. J. Zheng, W. L. Ng, R. W. M. Lai, Y. Guan, K. Y. Yuen; HKU/UCH SARS Study Group, Clinical progression and viral load in a community outbreak of coronavirus-associated SARS pneumonia: A prospective study. *Lancet* **361**, 1767–1772 (2003).
22. H. Yu, Z. Feng, T. M. Uyeki, Q. Liao, L. Zhou, L. Feng, M. Ye, N. Xiang, Y. Huai, Y. Yuan, H. Jiang, Y. Zheng, P. Gargiullo, Z. Peng, Y. Feng, J. Zheng, C. Xu, Y. Zhang, Y. Shu, Z. Gao, W. Yang, Y. Wang, Risk factors for severe illness with 2009 pandemic influenza A (H1N1) virus infection in China. *Clin. Infect. Dis.* **52**, 457–465 (2011).
23. M. D. Oh, W. B. Park, P. G. Choe, S. J. Choi, J. I. Kim, J. Chae, S. S. Park, E. C. Kim, H. S. Oh, E. J. Kim, E. Y. Nam, S. H. Na, D. K. Kim, S. M. Lee, K. H. Song, J. H. Bang, E. S. Kim, H. B. Kim, S. W. Park, N. J. Kim, Viral load kinetics of MERS coronavirus infection. *N. Engl. J. Med.* **375**, 1303–1305 (2016).
24. J. F. W. Chan, S. K. P. Lau, K. K. W. To, V. C. C. Cheng, P. C. Y. Woo, K.-Y. Yuen, Middle East respiratory syndrome coronavirus: Another zoonotic betacoronavirus causing SARS-like disease. *Clin. Microbiol. Rev.* **28**, 465–522 (2015).
25. D. Falzarano, E. de Wit, C. Martellaro, J. Callison, V. J. Munster, H. Feldmann, Inhibition of novel β coronavirus replication by a combination of interferon-α2b and ribavirin. *Sci. Rep.* **3**, 1686 (2013).
26. B. J. Hart, J. Dyall, E. Postnikova, H. Zhou, J. Kindrachuk, R. F. Johnson, G. G. Olinger Jr., M. B. Frieman, M. R. Holbrook, P. B. Jahrling, L. Hensley, Interferon-β and mycophenolic acid are potent inhibitors of Middle East respiratory syndrome coronavirus in cell-based assays. *J. Gen. Virol.* **95**, 571–577 (2014).
27. B. Morgenstern, M. Michaelis, P. C. Baer, H. W. Doerr, J. Cinatl Jr., Ribavirin and interferon-β synergistically inhibit SARS-associated coronavirus replication in animal and human cell lines. *Biochem. Biophys. Res. Commun.* **326**, 905–908 (2005).
28. N. Yamamoto, R. Yang, Y. Yoshinaka, S. Amari, T. Nakano, J. Cinatl, H. Rabenau, H. W. Doerr, G. Hunsmann, A. Otaka, H. Tamamura, N. Fujii, N. Yamamoto, HIV protease inhibitor nelfinavir inhibits replication of SARS-associated coronavirus. *Biochem. Biophys. Res. Commun.* **318**, 719–725 (2004).
29. J. F. Chan, K.-H. Chan, R. Y. T. Kao, K. K. W. To, B.-J. Zheng, C. P. Y. Li, P. T. W. Li, J. Dai, F. K. Y. Mok, H. Chen, F. G. Hayden, K.-Y. Yuen, Broad-spectrum antivirals for the emerging Middle East respiratory syndrome coronavirus. *J. Infect.* **67**, 606–616 (2013).
30. K. Ratia, S. Pegan, J. Takayama, K. Sleeman, M. Coughlin, S. Baliji, R. Chaudhuri, W. Fu, B. S. Prabhakar, M. E. Johnson, S. C. Baker, A. K. Ghosh, A. D. Mesecar, A noncovalent class of papain-like protease/deubiquitinase inhibitors blocks SARS virus replication. *Proc. Natl. Acad. Sci. U.S.A.* **105**, 16119–16124 (2008).
31. D. L. Barnard, C. W. Day, K. Bailey, M. Heiner, R. Montgomery, L. Lauridsen, S. Winslow, J. Hoopes, J. K.-K. Li, J. Lee, D. A. Carson, H. B. Cottam, R. W. Sidwell, Enhancement of the infectivity of SARS-CoV in BALB/c mice by IMP dehydrogenase inhibitors, including ribavirin. *Antiviral Res.* **71**, 53–63 (2006).
32. J. F.-W. Chan, Y. Yao, M.-L. Yeung, W. Deng, L. Bao, L. Jia, F. Li, C. Xiao, H. Gao, P. Yu, J.-P. Cai, H. Chu, J. Zhou, H. Chen, C. Qin, K.-Y. Yuen, Treatment with lopinavir/ritonavir or interferon-β1b improves outcome of MERS-CoV infection in a nonhuman primate model of common marmoset. *J. Infect. Dis.* **212**, 1904–1913 (2015).
33. A. S. Cockrell, B. L. Yount, T. Scobey, K. Jensen, M. Douglas, A. Beall, X.-C. Tang, W. A. Marasco, M. T. Heise, R. S. Baric, A mouse model for MERS coronavirus-induced acute respiratory distress syndrome. *Nat. Microbiol.* **2**, 16226 (2016).

34. M. Jacobs, A. Rodger, D. J. Bell, S. Bhagani, I. Cropley, A. Filipe, R. J. Gifford, S. Hopkins, J. Hughes, F. Jabeen, I. Johannessen, D. Karageorgopoulos, A. Lackenby, R. Lester, R. S. N. Liu, A. MacConnachie, T. Mahungu, D. Martin, N. Marshall, S. Mepham, R. Orton, M. Palmarini, M. Patel, C. Perry, S. E. Peters, D. Porter, D. Ritchie, N. D. Ritchie, R. A. Seaton, V. B. Sreenu, K. Templeton, S. Warren, G. S. Wilkie, M. Zambon, R. Gopal, E. C. Thomson, Late Ebola virus relapse causing meningoencephalitis: A case report. *Lancet* **388**, 498–503 (2016).

Acknowledgments: We would like to thank A. West and D. T. Scobey for excellent technical expertise. **Funding:** This study was funded by the Antiviral Drug Discovery and Development Center (5U19AI109680), grants from the NIH (AI108197 and AI109761), and the Cystic Fibrosis and Pulmonary Diseases Research and Treatment Center (BOUCHE15RO and NIH P30DK065988). Travel of M.R.D. to Gilead Sciences Inc. to discuss this project was paid for by Gilead Sciences. In addition, compound formulation and pharmacokinetic and metabolism studies were performed and paid for by Gilead Sciences. **Author contributions:** A.C.S., J.Y.F., T.P.S., T.C., R.J., and R.B. designed the in vitro efficacy studies. A.C.S., T.P.S., and S.R.L. executed and analyzed the in vitro efficacy studies. T.P.S., J.Y.F., R.J., T.C., R.S.B., and A.S.R. designed the in vivo efficacy studies. T.P.S. executed and analyzed the in vivo efficacy studies. R.B. scored the pathology and virus lung antigen staining. R.L.G. and K.P. performed qRT-PCR. V.D.M. and L.E.G. performed WBP for some in vivo studies. J.B.C. and M.R.D. designed and performed the pilot studies initially demonstrating efficacy against CoV. C.A.P., R.B., Y.P., D.B., and A.S.R., designed, executed, and analyzed the metabolism, pharmacokinetics, stability, or toxicity studies. M.O.C., D.S., R.L.M., J.E.S., and I.T. were responsible for the synthesis, scale-up, and formulation of small molecules. T.P.S., A.C.S., J.Y.F., T.C., R.S.B., M.R.D., D.B., R.J., and A.S.R. wrote the manuscript. **Competing interests:** The authors affiliated with Gilead Sciences are employees of the company and may own company stock. M.O.C., J.Y.F., R.J., R.L.M., A.S.R., and D.S. are listed as inventors on international application no. PCT/US2016/052092 filed by Gilead Sciences Inc., directed to methods of treating coronaviridae virus infections. All other authors declare that they have no competing interests. **Data and materials availability:** GS-5734 was made available to UNC under a materials transfer agreement with Gilead Sciences.

Submitted 8 November 2016
Accepted 17 May 2017
Published 28 June 2017
10.1126/scitranslmed.aal3653

Citation: T. P. Sheahan, A. C. Sims, R. L. Graham, V. D. Menachery, L. E. Gralinski, J. B. Case, S. R. Leist, K. Pyrc, J. Y. Feng, I. Trantcheva, R. Bannister, Y. Park, D. Babusis, M. O. Clarke, R. L. Mackman, J. E. Spahn, C. A. Palmiotti, D. Siegel, A. S. Ray, T. Cihlar, R. Jordan, M. R. Denison, R. S. Baric, Broad-spectrum antiviral GS-5734 inhibits both epidemic and zoonotic coronaviruses. *Sci. Transl. Med.* **9**, eaal3653 (2017).

Science Translational Medicine

Broad-spectrum antiviral GS-5734 inhibits both epidemic and zoonotic coronaviruses

Timothy P. Sheahan, Amy C. Sims, Rachel L. Graham, Vineet D. Menachery, Lisa E. Gralinski, James B. Case, Sarah R. Leist, Krzysztof Pyrc, Joy Y. Feng, Iva Trantcheva, Roy Bannister, Yeojin Park, Darius Babusis, Michael O. Clarke, Richard L. Mackman, Jamie E. Spahn, Christopher A. Palmiotti, Dustin Siegel, Adrian S. Ray, Tomas Cihlar, Robert Jordan, Mark R. Denison and Ralph S. Baric

Sci Transl Med **9**, eaal3653.
DOI: 10.1126/scitranslmed.aal3653

Antiviral gets the jump on coronaviruses

Like other emerging infections, coronaviruses can jump from animal reservoirs into the human population with devastating effects, such as the SARS or MERS outbreaks. Sheahan *et al*. tested a small-molecule inhibitor that has shown activity against Ebola virus as a potential agent to be used to fight coronaviruses. This drug was effective against multiple types of coronaviruses in cell culture and in a mouse model of SARS and did not seem to be toxic. Given its broad activity, this antiviral could be deployed to prevent spreading of a future coronavirus outbreak, regardless of the specific virus that jumps over.

Science Translational Medicine (ISSN 1946-6242) is published by the American Association for the Advancement of Science, 1200 New York Avenue NW, Washington, DC 20005. The title *Science Translational Medicine* is a registered trademark of AAAS.